

RS-RAG: Bridging Remote Sensing Imagery and Comprehensive Knowledge with a Multi-Modal Dataset and Retrieval-Augmented Generation Model

Congcong Wen *Member, IEEE*, Yiting Lin, Xiaokang Qu, Nan Li, Yong Liao, Hui Lin, and Xiang Li

Abstract—Recent progress in Vision-Language Models (VLMs) has demonstrated impressive capabilities across a variety of tasks in the natural image domain. Motivated by these advancements, the remote sensing community has begun to adopt VLMs for remote sensing vision-language tasks, including scene understanding, image captioning, and visual question answering. However, existing remote sensing VLMs typically rely on closed-set scene understanding and focus on generic scene descriptions, yet lack the ability to incorporate external knowledge. This limitation hinders their capacity for semantic reasoning over complex or context-dependent queries that involve domain-specific or world knowledge. To address these challenges, we first introduced a multimodal Remote Sensing World Knowledge (RSWK) dataset, which comprises high-resolution satellite imagery and detailed textual descriptions for 14,141 well-known landmarks from 175 countries, integrating both remote sensing domain knowledge and broader world knowledge. Building upon this dataset, we proposed a novel Remote Sensing Retrieval-Augmented Generation (RS-RAG) framework, which consists of two key components. The Multi-Modal Knowledge Vector Database Construction module encodes remote sensing imagery and associated textual knowledge into a unified vector space. The Knowledge Retrieval and Response Generation module retrieves and re-ranks relevant knowledge based on image and/or text queries, and incorporates the retrieved content into a knowledge-augmented prompt to guide the VLM in producing contextually grounded responses. We validated the effectiveness of our approach on three representative vision-language tasks, including image captioning, image classification, and visual question answering, where RS-RAG significantly outperformed state-of-the-art baselines. By bridging remote sensing imagery and comprehensive knowledge, RS-RAG empowers remote sensing VLMs with enhanced contextual reasoning, enabling them to generate more accurate, informative, and semantically grounded outputs across a wide range of tasks.

Index Terms—Remote Sensing, Vision Language Model, Retrieval-Augmented Generation, World Knowledge

This work was partly supported by the Beijing Nova Program under Grant 2024124 and the National Natural Science Foundation of China under Grant U24B20177. (Congcong Wen and Yiting Lin contributed equally to this work). (Corresponding author: Hui Lin).

Congcong Wen, Yiting Lin, Xiaokang Qu and Yong Liao are with School of Cyber Science and Technology, University of Science and Technology of China, Anhui, 230026, China. Congcong Wen is also with the Department of Electrical and Computer Engineering, New York University Abu Dhabi, Abu Dhabi, UAE. (e-mail: wencec1208@gmail.com, linyiting@mail.ustc.edu.cn, xkqu@mail.ustc.edu.cn and ylliao@ustc.edu.cn)

Nan Li and Hui Lin are with China Academy of Electronics and Information Technology, Beijing 100846, China. (e-mail: linhui@whu.edu.cn and nli2014@lzu.edu.cn)

Xiang Li is with the Department of Computer Science at the University of Reading, Reading RG6 6AH, UK. (e-mail: xiangli92@ieee.org)

I. INTRODUCTION

Remote sensing imagery, as a critical source of information for Earth observation and monitoring, plays an essential role in urban planning [1], agricultural assessment [2], and environmental protection [3]. However, as remote sensing technology advances, the scale and complexity of imagery data have rapidly increased, making it increasingly difficult for traditional manual analysis or image processing methods to meet practical demands. Deep learning methods [4], [5] have significantly improved the accuracy and efficiency of tasks like classification, segmentation and object detection by automatically extracting features from vast amounts of remote sensing data. While these methods have made notable progress, most deep learning models rely predominantly on single-modal visual information, lacking deep semantic understanding of image content. This limitation results in reduced generalization and adaptability, particularly for tasks that require in-depth semantic analysis and comprehensive scene understanding.

The emergence of Vision-Language Models (VLMs) [6], [7], [8], [9], [10], [11] offers a novel solution for the semantic analysis of remote sensing data. By leveraging multimodal fusion techniques, VLMs combine visual features with language information to automatically generate descriptive insights for remote sensing imagery. This semantic enhancement improves image classification and object detection performance while enabling the transformation of recognition results into natural language descriptions, making them more interpretable and accessible for various applications. Additionally, VLMs perform well even in weakly supervised or zero-shot learning scenarios, providing reliable analysis with limited labeled data and thus reducing dependency on extensive data annotations. This cross-modal integration not only enhances the model's cognitive ability to interpret remote sensing imagery but also facilitates detailed semantic descriptions of complex scenes, paving the way for broader intelligent applications in remote sensing. However, existing remote sensing VLMs primarily focus on identifying image features and providing basic scene descriptions, lacking deeper background understanding of the objects within the images. Particularly when it comes to rich semantic information requiring remote sensing domain expertise or other general world knowledge, such as historical, cultural, and social contexts, these VLM models often struggle to provide comprehensive contextual support.

To address this issue, we first introduce the Remote Sensing World Knowledge (RSWK) dataset, a multimodal remote sens-

ing dataset that contains high-resolution imagery and natural language descriptions for approximately 14,141 well-known locations worldwide from 175 countries. Unlike most existing remote sensing vision-language datasets that only provide basic descriptions of current scenes, our RSWK dataset will include richer remote sensing domain expertise and world knowledge about the objects within these scenes. For instance, from a remote sensing perspective, it will provide information on surface reflectance, spectral indices, and atmospheric. From a world knowledge perspective, it will include historical background, cultural significance, construction period, and major events. This combination of remote sensing expertise and world knowledge will not only enhance the RSWK dataset's utility for visual analysis of remote sensing images, but also provide the model with deeper semantic context, overcoming the limitations of traditional datasets and enabling remote sensing VLMs to perform more complex cognitive tasks. Furthermore, our dataset incorporates historical, cultural, and social backgrounds from various countries and regions, allowing VLM models to be trained across diverse geographical and cultural contexts, thereby improving their generalization ability and understanding of different cultural settings.

Furthermore, to effectively leverage the comprehensive information provided by the RSWK dataset, we propose the Remote Sensing Retrieval-Augmented Generation (RS-RAG) model. RS-RAG is designed to enhance the capacity of vision-language models to generate contextually enriched and knowledge-grounded responses for remote sensing imagery. It operates by integrating external knowledge, both domain-specific and general world knowledge, retrieved from a multimodal knowledge base constructed using the RSWK dataset. The model consists of two main components: (1) the Multi-Modal Knowledge Vector Database Construction module, which encodes satellite imagery and textual descriptions into a shared embedding space using unified image and text encoders to enable efficient cross-modal retrieval; and (2) the Knowledge Retrieval and Response Generation module, which retrieves top-ranked knowledge entries based on image and text queries, re-ranks them via a fused similarity score, and incorporates the selected content into a knowledge-augmented prompt. This prompt is then passed to the vision-language model, enabling it to generate responses that go beyond semantic understanding and reflect deeper background knowledge. By coupling visual input with relevant contextual information, RS-RAG significantly improves the interpretability and accuracy of vision-language outputs, particularly for complex queries involving geospatial, historical, or environmental reasoning. To assess the effectiveness of our proposed model, we construct a lightweight benchmark and conduct comprehensive experiments on three representative tasks: image captioning, image classification, and visual question answering. Results on these tasks demonstrate the model's ability to produce accurate, context-rich descriptions, deliver semantically informed scene classifications, and provide precise answers to knowledge-intensive queries by leveraging both visual and textual modalities. Through these findings, RS-RAG demonstrates its potential to substantially advance the capabilities of vision-language models in remote sensing, ef-

fectively bridging the gap between imagery and comprehensive contextual knowledge. Our main contributions are summarized as follows:

- We construct the Remote Sensing World Knowledge (RSWK) dataset, a large-scale multimodal benchmark containing 14,141 high-resolution remote sensing images and rich textual descriptions of globally recognized landmarks from 175 countries. The descriptions incorporate both domain-specific knowledge (e.g., land use, temperature, wind direction) and general world knowledge (e.g., historical, cultural, and societal context).
- We propose RS-RAG, a novel Retrieval-Augmented Generation framework tailored for remote sensing vision-language tasks. RS-RAG retrieves semantically relevant knowledge from a multimodal vector database and integrates it with the input via knowledge-conditioned prompt construction, significantly enhancing contextual reasoning capabilities.
- We design a lightweight benchmark for evaluating remote sensing vision-language models across three core tasks: image captioning, image classification, and visual question answering. This benchmark enables systematic assessment of both semantic understanding and deeper knowledge-grounded reasoning.
- Extensive experiments demonstrate that RS-RAG consistently outperforms state-of-the-art vision-language models across all tasks, particularly on queries requiring external world knowledge. These results highlight the effectiveness of RS-RAG in bridging remote sensing imagery with structured knowledge, and point to promising future directions for research on remote sensing vision-language models.

II. RELATED WORK

A. Remote Sensing Multimodal Datasets

Several multimodal datasets [12], [13], [14], [15], [16] have been developed to bridge the gap between vision and language in the remote sensing domain. UCM Captions [17], Sydney Captions [17], and RSICD [18] are among the earliest datasets that provide textual descriptions for remote sensing images. Each image in these datasets is paired with five relatively simple human-written sentences, offering only a basic level of semantic information. To enhance the quality and richness of textual annotations, RSGPT [6] recently introduced RSICap, a high-quality image captioning dataset with detailed human-annotated descriptions of aerial scenes. RSICap serves as a valuable resource for fine-tuning and developing domain-specific vision-language models in remote sensing. Beyond manual annotation, researchers have explored the construction of large-scale datasets using automatic or hybrid approaches applied to existing data sources. For instance, RS5M [19] was created by aggregating 11 publicly available image-text paired datasets along with three large-scale class-level labeled datasets. Captions were generated using BLIP-2, resulting in a diverse and large-scale dataset suitable for training foundational multimodal models. Similarly, RemoteCLIP [20]

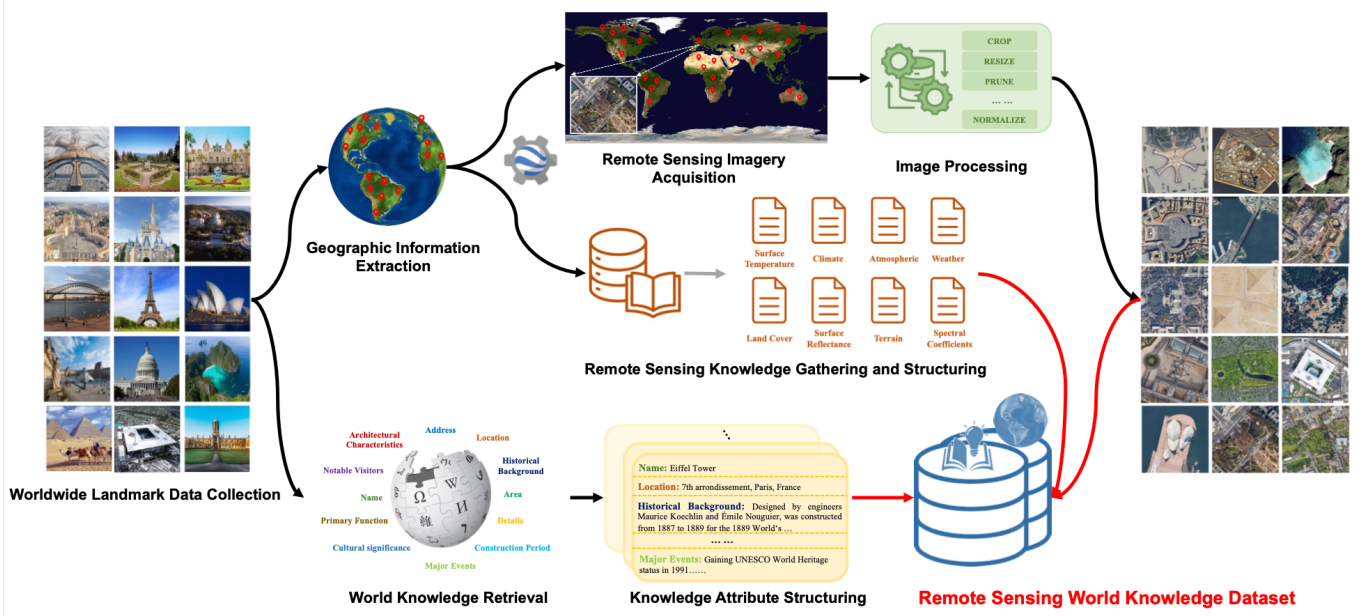


Fig. 1. The construction process of the Remote Sensing World Knowledge (RSWK) dataset begins with collecting landmark data from around the world, followed by extracting geographic information to pinpoint precise location coordinates. Using these coordinates, remote sensing images are acquired, which are further standardized through image processing techniques. Corresponding remote sensing expert knowledge, such as surface temperature, climate, atmospheric conditions, and spectral coefficients, is also included. Additionally, world knowledge is retrieved from online resources, providing detailed background information about the landmarks, including historical context, cultural significance, and major events. This combined information is structured into organized attributes to align image and text data, forming a final multimodal dataset. The resulting RSWK dataset integrates high-resolution images with extensive remote sensing and world knowledge, enabling advanced semantic understanding in remote sensing applications.

compiled a large-scale dataset by integrating 10 object detection datasets, 4 semantic segmentation datasets, and 3 remote sensing image–text datasets, enabling contrastive pretraining for cross-modal alignment. In addition, GeoChat introduced the RS Multimodal Instruction Dataset, which incorporates heterogeneous data sources, including three object detection datasets, one scene classification dataset, and a visual question answering dataset focused on flood detection. More recently, FedRSCLIP [21] proposed a new multimodal remote sensing dataset specifically designed for federated learning scenarios, further expanding the applicability of vision-language research in distributed settings. These efforts collectively advance the development of remote sensing VLMs by providing diverse, rich, and large-scale multimodal data resources tailored to various downstream tasks.

B. Remote Sensing Multimodal Model

With the growing availability of remote sensing multimodal datasets, a number of vision-language models [6], [7], [8], [9], [10], [11] have been proposed to enhance the understanding and interpretation of aerial imagery through natural language. [22] provides the first comprehensive review of vision-language models in remote sensing, systematically summarizing tasks, datasets, and methods, and identifying key challenges and future directions. RSCLIP [23] is a pioneering vision-language model designed for remote sensing scene classification, which leverages contrastive vision-language supervision and incorporates a pseudo-labeling technique along with a curriculum learning strategy to improve zero-shot classification performance through multi-stage fine-tuning. RSGPT [6]

represents one of the earliest attempts to build a generative pretrained model for remote sensing. It fine-tunes only the Q-Former and a linear projection layer on the proposed RSI-Cap dataset, achieving notable improvements in both image captioning and visual question answering tasks. Similarly, GeoChat [24] adapts the LLaVA-1.5 architecture and fine-tunes it on its proposed remote sensing multimodal instruction-following dataset, offering multi-task conversational capabilities grounded in high-resolution satellite imagery. In addition, to address the common issue of hallucination in remote sensing vision-language models, a Helpful and Honest Remote Sensing Vision-Language Model [8], named H2RSVLM, is proposed and fine-tuned on the RSSA dataset, the first dataset specifically designed to enhance self-awareness in remote sensing VLMs. More recently, RSMoE [25] was proposed as the first Mixture-of-Experts-based VLM tailored for remote sensing. It features a novel instruction router that dynamically dispatches tasks to multiple lightweight expert LLMs, allowing each expert to specialize in a specific subset of tasks.

III. DATASET CONSTRUCTION

Most existing remote sensing VLM datasets focus primarily on basic descriptions of objects in a scene, typically providing only information about the objects present. While these datasets serve a purpose in supporting fundamental tasks such as scene classification and image captioning, they fall short in applications requiring complex semantic understanding or contextual awareness. To address this limitation, in our full paper, we would like to propose the Remote Sensing World Knowledge (RSWK) dataset, which encompasses high-resolution

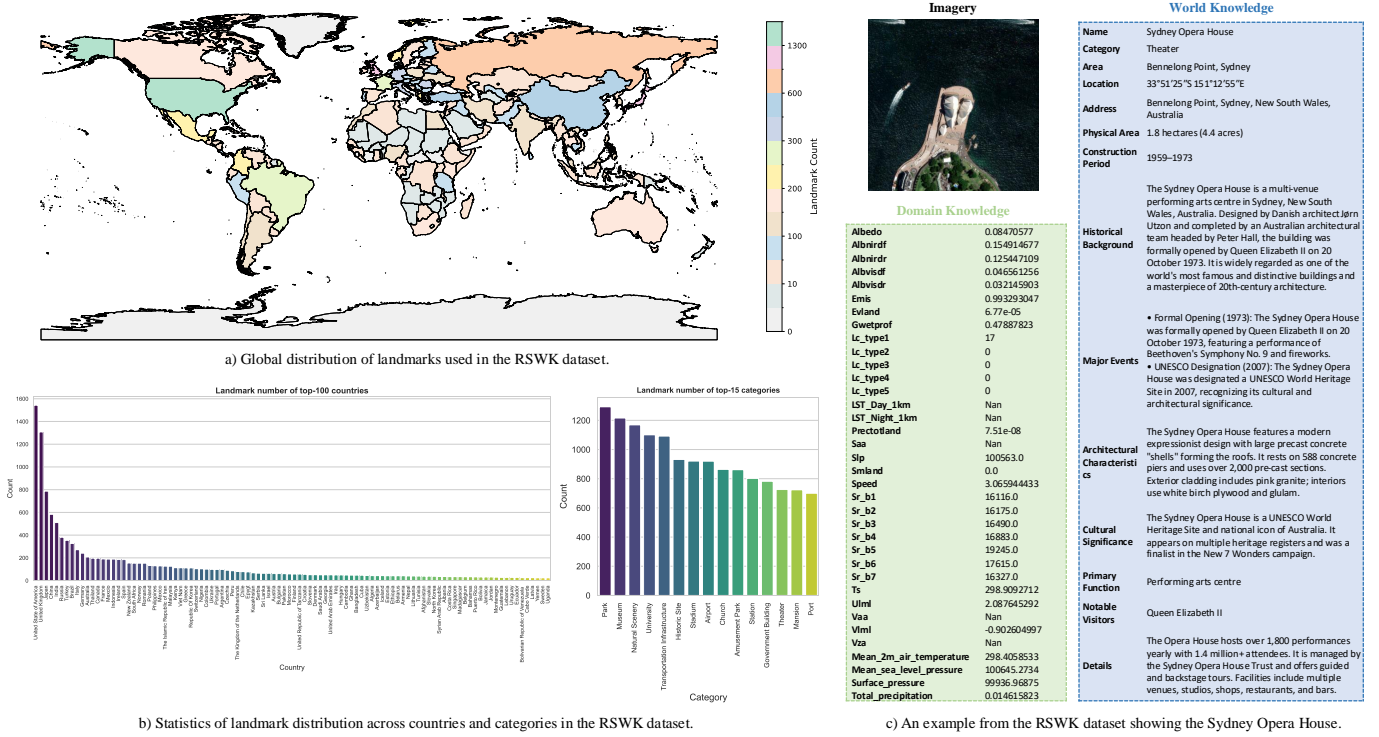


Fig. 2. Overview of the RSWK dataset. (a) Global distribution of landmarks used in the dataset, with color indicating the number of landmarks per country. (b) Statistical summaries of landmark counts across the top 100 countries (left) and the top 15 most frequent landmark categories (right). (c) A specific example from the RSWK dataset, showcasing the Sydney Opera House, including its satellite imagery, remote sensing domain knowledge, and structured world knowledge.

remote sensing imagery of well-known locations worldwide, along with domain knowledge and world knowledge described in natural language. This dataset not only fills the gap in knowledge depth and breadth found in current remote sensing datasets but also provides a new foundation for advancing remote sensing technology toward intelligent applications. The core value of remote sensing data lies in its ability to deliver rich geographic and spatial distribution information. By integrating high-resolution imagery from across the globe with detailed domain knowledge and world knowledge, the RSWK dataset extends this value, expanding the application of remote sensing data from traditional foundational tasks to complex scenarios that require deeper semantic understanding.

A. Data Processing

Fig. 1 illustrates the end-to-end pipeline for constructing the Remote Sensing World Knowledge (RSWK) dataset, which aims to bridge the gap between remote sensing domain knowledge and encyclopedic world knowledge of globally distributed landmarks. This pipeline is designed to automatically curate and align multimodal information from global sources, integrating high-resolution remote sensing imagery, remote sensing expert knowledge, and contextual world knowledge. The process begins with GPT-4o [26], a state-of-the-art large language model, which is employed to generate a comprehensive list of globally recognized landmarks across diverse countries and regions, ensuring broad cultural and geographic coverage that includes both natural and man-made sites of

historical and societal relevance. To acquire world knowledge, we utilize the Wikipedia API to extract descriptive information for each landmark, such as historical background, cultural relevance, architectural details, and notable events, with the complete set of fields shown in Table I. Post-processing is performed using DeepSeek [27] to remove low-quality or irrelevant entries. In parallel, the Google Geocoding API is used to obtain precise geographic coordinates for each location; to resolve potential ambiguities in place names, we implement a validation mechanism that cross-references multiple sources and applies regional constraints. High-resolution satellite imagery is retrieved from the ArcGIS Tile Map Service, with spatial resolutions ranging from 0.6m to 0.15m, followed by normalization, cropping, and resizing to ensure consistency in image quality and dimensions. Concurrently, remote sensing expert knowledge is derived using Google Earth Engine (GEE) [28], as detailed in Table II. This includes a wide range of satellite-derived geophysical and meteorological variables such as land surface temperature, surface albedo, land cover classification, vegetation indices, and precipitation, which are sourced from authoritative datasets like MODIS, Landsat, and ERA5. By integrating these three complementary modalities, remote sensing imagery, remote sensing expert knowledge, and contextual world knowledge, the RSWK dataset provides a rich foundation for multimodal learning in remote sensing, enabling downstream tasks such as image captioning, image classification, and visual question answering.

TABLE I
WORLD KNOWLEDGE FIELDS AND DESCRIPTIONS FOR LANDMARK IN
THE RSWK DATASET.

Field Name	Description
Name	The official or commonly known name of the landmark.
Category	The type of the landmark.
Area	The general geographical region or country where the landmark is located.
Location	Latitude and longitude coordinates of the landmark.
Address	Full postal or descriptive address of the landmark.
Physical_Area	The spatial footprint or size of the landmark.
Construction_Period	The years or range of years during which the landmark was constructed.
Historical_Background	Historical context, including origin, founding date, and development over time.
Major_Events	Key historical or cultural events that occurred at the landmark.
Architectural_Characteristics	Notable features such as design style, construction materials, and structure.
Cultural_Significance	The cultural, symbolic, or religious importance of the landmark.
Primary_Function	The main use or role of the landmark (e.g., tourist attraction, government building).
Notable_Visitors	Famous individuals or groups who have visited the site.
Details	Additional facts or interesting information not captured by other fields.

TABLE II
REMOTE SENSING DOMAIN KNOWLEDGE FIELDS, DESCRIPTIONS, AND
SOURCE FOR LANDMARK IN THE RSWK DATASET.

Field Name	Description	Source
Albedo	Surface albedo, representing the reflectivity of the Earth's surface	MERRA-2 (M2T1NXRAD)
Albnirdf	Near-infrared diffuse surface albedo	MERRA-2 (M2T1NXRAD)
Albnirdr	Near-infrared direct surface albedo	MERRA-2 (M2T1NXRAD)
Albnisdr	Visible light direct albedo	MERRA-2 (M2T1NXRAD)
Albnisdr	Visible light direct albedo	MERRA-2 (M2T1NXRAD)
Emis	Surface emissivity, related to thermal radiation	MERRA-2 (M2T1NXRAD)
Evland	Evaporation land (kg/m ² /s)	MERRA-2 (M2T1NXLND)
Gwetprof	Profile soil moisture averaged over depth	MERRA-2 (M2T1NXLND)
LC_type1	Land cover type (IGBP classification)	MODIS (MCD12Q1.061)
LC_type2	Land cover type (UMD classification)	MODIS (MCD12Q1.061)
LC_type3	Land cover type (LAI classification)	MODIS (MCD12Q1.061)
LC_type4	Land cover type (BGC classification)	MODIS (MCD12Q1.061)
LC_type5	Land cover type (Plant Functional Types classification)	MODIS (MCD12Q1.061)
LST_Day_1km	Daytime land surface temperature (°C)	MODIS (MOD11A1.061)
LST_Night_1km	Nighttime land surface temperature (°C)	MODIS (MOD11A1.061)
Prcetotland	Total land precipitation (kg/m ² /s)	MERRA-2 (M2T1NXLND)
Saa	Sun Azimuth Angle (°)	HLSL30 (HLS-2)
Slp	Sea level pressure (Pa)	MERRA-2 (M2T1NXSLV)
Smland	Snowmelt flux land (kg/m ² /s)	MERRA-2 (M2T1NXLND)
Speed	Surface wind speed (m/s)	MERRA-2 (M2T1NXFLX)
Sr_b1	Band 1 (ultra blue, coastal aerosol) surface reflectance	Landsat 9
Sr_b2	Band 2 (blue) surface reflectance	Landsat 9
Sr_b3	Band 3 (green) surface reflectance	Landsat 9
Sr_b4	Band 4 (red) surface reflectance	Landsat 9
Sr_b5	Band 5 (near infrared) surface reflectance	Landsat 9
Sr_b6	Band 6 (shortwave infrared 1) surface reflectance	Landsat 9
Sr_b7	Band 7 (shortwave infrared 2) surface reflectance	Landsat 9
Ts	Surface skin temperature (°C)	MERRA-2 (M2T1NXSLV)
U1ml	Surface eastward wind (m/s)	MERRA-2 (M2T1NXFLX)
Vaa	View Azimuth Angle (°)	HLSL30 (HLS-2)
V1ml	Surface northward wind speed (m/s)	MERRA-2 (M2T1NXFLX)
Vza	View Zenith Angle (°)	HLSL30 (HLS-2)
Mean_2m_air_temperature	Average air temperature at 2m height (°C)	ERA5 (Daily Aggregates)
Mean_sea_level_pressure	Mean sea level pressure (Pa)	ERA5 Daily Aggregates
Surface_pressure	Surface pressure (Pa)	ERA5 (Daily Aggregates)
Total_precipitation	Total precipitation (m)	ERA5 (Daily Aggregates)

B. Data Statistics

Through the above data construction pipeline, the RSWK dataset successfully collected a total of 14,141 landmark instances from 175 countries, each accompanied by high-resolution satellite imagery, domain-specific remote sensing attributes, and structured world knowledge descriptions. The global spatial distribution of the landmarks is visualized in Fig. 2(a), demonstrating wide coverage across all major continents. Notably, the dataset includes landmarks from a diverse range of regions, effectively covering most major countries worldwide. To provide a more detailed view of the dataset composition, we present the distribution of landmarks across the top 100 countries sorted by landmark count in Fig. 2(b, left). It can be observed that countries such as the United

States, the United Kingdom, China, and Japan contribute the largest number of landmarks. This reflects both the cultural richness and the degree of documentation available for landmarks in these regions. In addition, Fig. 2(b, right) shows the frequency distribution of the top 15 landmark categories, including parks, museums, natural scenery, universities, and historic sites. The category distribution is relatively balanced, highlighting the diverse types of landmarks captured in the dataset and ensuring a rich set of semantic concepts for downstream tasks. To provide an intuitive example of how the data is structured, we present the Sydney Opera House in Fig. 2(c) as a representative landmark. The figure illustrates the three core components of each RSWK entry: the satellite imagery, the domain knowledge (e.g., albedo, emissivity, land cover type, and meteorological variables), and the structured world knowledge (e.g., historical background, architectural characteristics, and cultural significance). This tri-modal representation demonstrates the depth and richness of the dataset, supporting a wide range of geospatial understanding and vision-language reasoning tasks.

IV. METHODOLOGY

To bridge the semantic gap between remote sensing imagery and comprehensive external knowledge, we propose RS-RAG, a Retrieval-Augmented Generation framework designed to integrate both domain-specific and world knowledge into vision-language reasoning. As illustrated in Fig. 3, RS-RAG consists of two main components: the *Multi-Modal Knowledge Vector Database Construction* module, which encodes remote sensing imagery and textual knowledge into a unified embedding space; and the *Knowledge Retrieval and Response Generation* module, which retrieves and fuses the most relevant knowledge to support downstream tasks. By conditioning the vision-language model on retrieved context, RS-RAG enables knowledge-grounded understanding for diverse applications such as image captioning, scene classification, and visual question answering.

A. Problem Formulation

VLMs are designed to generate natural language outputs conditioned on multimodal inputs, typically a visual observation and a textual prompt. Let q_I denote the input image (e.g., a remote sensing image), and q_T the associated textual prompt (e.g., a question or instruction). A conventional VLM seeks to generate a natural language response \hat{y} by modeling the conditional probability distribution over output space and selecting the most probable response. Formally, this can be expressed as:

$$\hat{y} = \arg \max_y P(y \mid q_T, q_I; \theta_{\text{VLM}}), \quad (1)$$

where θ_{VLM} represents the parameters of the VLM, \hat{y} can represent an image caption, a classification label, or an answer to a visual question. This closed-form generation framework assumes that all necessary information for reasoning is either visually grounded in the input image q_I or implicitly encoded within the model parameters θ_{VLM} . While this assumption often holds for natural image datasets, it becomes problematic

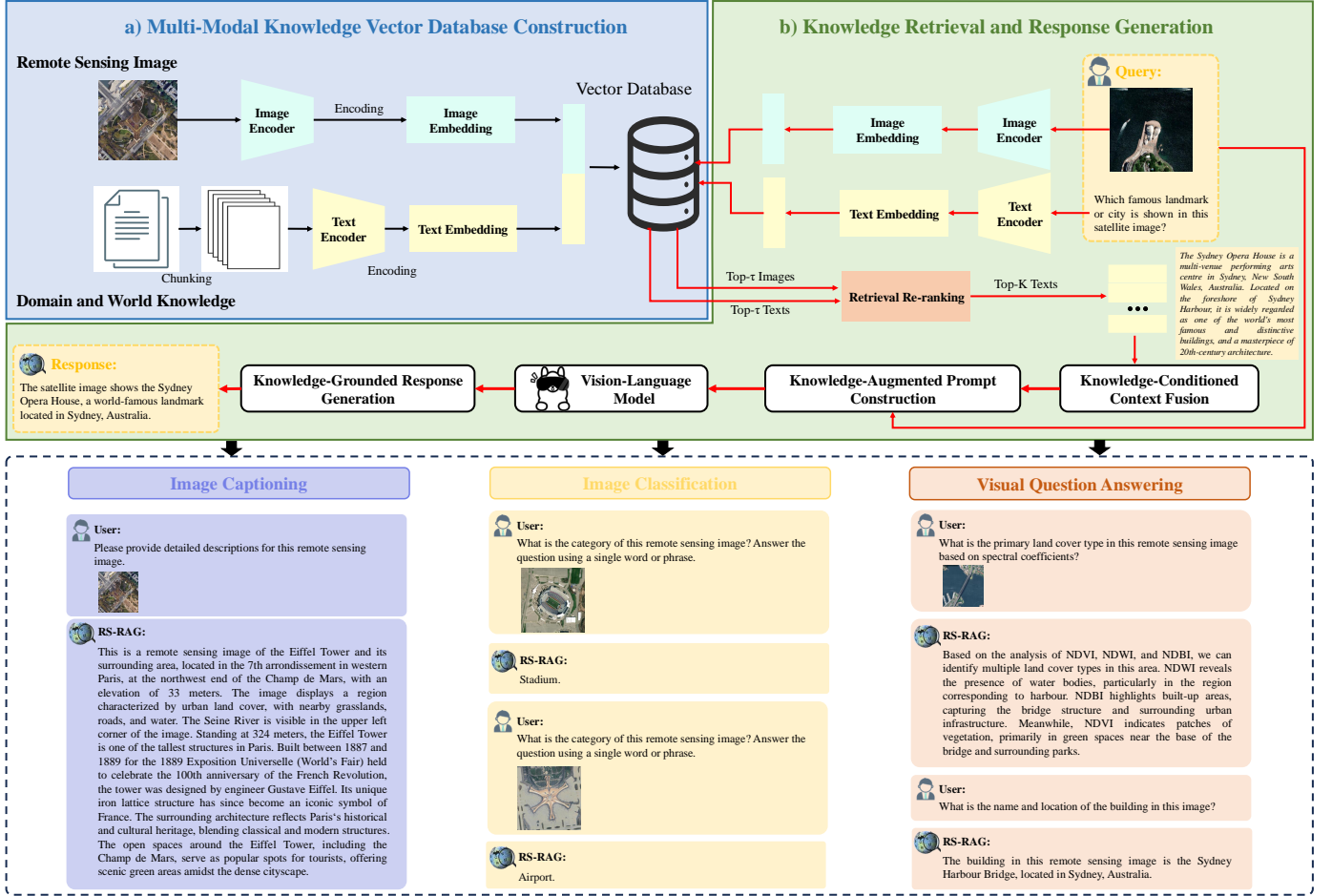


Fig. 3. Overview of the proposed Remote Sensing Retrieval-Augmented Generation (RS-RAG) model. It consists of two main processes: (a) The Multi-Modal Knowledge Vector Database Construction module encodes remote sensing imagery and domain/world knowledge into a unified vector space via image and text encoders, enabling efficient cross-modal retrieval. (b) The Knowledge Retrieval and Response Generation module retrieves top-k relevant knowledge based on image and/or textual queries, and re-ranks the results for better relevance. Retrieved knowledge is fused into the prompt through Knowledge-Conditioned Context Fusion, guiding the Vision-Language Model (VLM) to generate Knowledge-Grounded Responses. The RS-RAG model supports multiple downstream tasks such as Image Captioning, Image Classification, and Visual Question Answering, as demonstrated in the bottom section.

in the domain of remote sensing. Remote sensing images typically capture large-scale scenes, such as entire cities or extensive geographic regions, where accurate interpretation often relies on understanding cultural, historical, or geographical significance. Such knowledge is rarely discernible from visual features and is not explicitly modeled in conventional VLMs.

To address this limitation, we extend the standard VLM formulation by incorporating external, query-relevant knowledge. Specifically, we adopt a Retrieval-Augmented Generation (RAG) framework, wherein a set of top- k relevant knowledge snippets \mathbf{R} is retrieved from an external corpus based on the multimodal similarity between the input image-text pair (q_I, q_T) and the knowledge index. The retrieved context \mathbf{R} is then integrated with the original inputs to guide the response generation process. Formally, the objective becomes:

$$\hat{y} = \arg \max_y P(y \mid q_T, q_I, \mathbf{R}; \theta_{\text{VLM}}), \quad (2)$$

where the additional context \mathbf{R} allows the model to produce more informative and contextually grounded outputs. This open-book generation paradigm is particularly well-suited for remote sensing applications, where high-level semantic

understanding often depends on both domain-specific knowledge (e.g., land use categories) and broader world knowledge (e.g., cultural or geopolitical significance)—information that is typically absent from raw pixel data alone.

B. Multi-Modal Knowledge Vector Database Construction

To enable retrieval-augmented generation, we construct a Multi-Modal Knowledge Vector Database (MKVD) by encoding the RSWK dataset, which contains high-resolution remote sensing images I_i and their paired textual descriptions T_i . These data are transformed into dense embeddings using CLIP and stored in a shared semantic space to support efficient and flexible cross-modal retrieval. We adopt CLIP as a unified encoder consisting of a image encoder $f_I(\cdot)$ and a text encoder $f_T(\cdot)$, each mapping input into a shared embedding space \mathbb{R}^d . Each image I_i is encoded into a visual embedding:

$$\mathbf{v}_i = f_I(I_i) \in \mathbb{R}^d. \quad (3)$$

In parallel, the corresponding textual document T_i is segmented into m_i semantically coherent chunks

$\{T_{i,1}, T_{i,2}, \dots, T_{i,m_i}\}$, and each chunk is encoded using the text encoder:

$$\mathbf{t}_{i,j} = f_T(T_{i,j}) \in \mathbb{R}^d. \quad (4)$$

The resulting image embeddings $\{\mathbf{v}_i\}$ and text embeddings $\{\mathbf{t}_{i,j}\}$ are indexed in Qdrant, a high-performance vector database optimized for approximate nearest neighbor (ANN) search. To organize the data, embeddings are stored in two separate collections: $\mathcal{D}_{\text{image}}$ for image embeddings and $\mathcal{D}_{\text{text}}$ for text embeddings. Each image-text pair is linked via a unique identifier ID_i . Specifically, each $\mathbf{v}_i \in \mathcal{D}_{\text{image}}$ is associated with a set $\{\mathbf{t}_{i,j}\}_{j=1}^{m_i} \subset \mathcal{D}_{\text{text}}$, which encodes domain-specific and general world knowledge about the same location or object. Metadata such as raw textual descriptions, image paths, and geospatial attributes are stored alongside each entry as payloads. This database structure supports modality-specific and cross-modal retrieval, serving as the foundation for external knowledge integration in the RS-RAG framework.

C. Knowledge Retrieval and Response Generation

After constructing the Multi-Modal Knowledge Vector Database, we implement a retrieval-augmented generation pipeline that enhances vision-language understanding by incorporating external knowledge retrieved via cross-modal similarity. Given a user query q , composed of an image component q_I and a textual component q_T , we first encode each input into dense embeddings:

$$\mathbf{v}_T = f_T(q_T), \quad \mathbf{v}_I = f_I(q_I), \quad (5)$$

where $f_T(\cdot)$ and $f_I(\cdot)$ denote the CLIP-based text and image encoders, respectively. To retrieve semantically relevant knowledge, we perform similarity search in both the text and image embedding spaces, retrieving the top- τ candidates from each modality:

$$\mathcal{R}_T^\tau = \text{Top}_\tau(\mathbf{v}_T, \mathcal{D}_{\text{text}}), \quad \mathcal{R}_I^\tau = \text{Top}_\tau(\mathbf{v}_I, \mathcal{D}_{\text{image}}), \quad (6)$$

where $\mathcal{D}_{\text{text}}$ and $\mathcal{D}_{\text{image}}$ represent the text and image embedding collections in the vector database. While the initial retrieval from each modality yields candidates based on unimodal similarity, these results may contain semantically redundant, irrelevant, or inconsistent entries due to the disjoint nature of visual and textual embedding spaces. To address this issue, we introduce a *retrieval re-ranking* step that jointly considers both modalities. Specifically, we first merge the retrieved sets from each modality, $\mathcal{R}_{\text{fused}} = \mathcal{R}_T^\tau \cup \mathcal{R}_I^\tau$. Each candidate is then assigned a fused similarity score via weighted combination:

$$\text{score}(r_i) = (1 - \alpha) \cdot s_T(r_i) + \alpha \cdot s_I(r_i), \quad (7)$$

where $s_{\text{text}}(r_i)$ and $s_{\text{image}}(r_i)$ are the cosine similarities between the query and the candidate in the respective embedding spaces. The weighting parameter $\alpha \in [0, 1]$ controls the relative influence of each modality. Based on these fused scores, we select the top- K most relevant candidates:

$$\{k_1, \dots, k_K\} = \text{Top}_K(\{\text{score}(r_i) \mid r_i \in \mathcal{R}_{\text{fused}}\}). \quad (8)$$

To enhance semantic coherence and eliminate redundancy among the retrieved segments, we apply a *Knowledge-Conditioned Context Fusion* module that consolidates them

into a single, contextually grounded representation. Specifically, a frozen large language model $\mathcal{L}_{\text{fuse}}$ is employed to synthesize the knowledge-conditioned context \mathbf{R} from the top-ranked knowledge snippets:

$$\mathbf{R} = \mathcal{L}_{\text{fuse}}(\{k_1, \dots, k_K\}). \quad (9)$$

This fusion step consolidates salient content from the retrieved segments into a compact, context-aware representation, thereby facilitating structured prompt construction. Given the original user query q_T and the fused knowledge context \mathbf{R} , we construct a retrieval-augmented prompt P_q via *Knowledge-Augmented Prompt Construction* as follows:

$$P_q = \text{Concat}[\phi, q_T, \psi, \mathbf{R}] \quad (10)$$

where ϕ is a task-specific instruction token (e.g., “Answer the following question based on the retrieved knowledge:”), ψ is a knowledge header (e.g., “Retrieved context:”), and \mathbf{R} is the fused knowledge used to support reasoning. Finally, the composed prompt P_q , along with the visual input q_I , is provided to the VLM, which performs Knowledge-Grounded Response Generation via joint multimodal reasoning and generates the final output:

$$\hat{y} = \text{Generate}_{\theta_{\text{VLM}}}(y \mid \text{Image} = q_I, \text{Prompt} = P_q). \quad (11)$$

By leveraging retrieval from a multi-modal knowledge base, this framework empowers the RS-VLMs to go beyond purely visual grounding by integrating both domain-specific knowledge and broader world knowledge, including cultural, historical, and geopolitical context. This enriched understanding enables the model to generate more accurate, context-aware, and semantically comprehensive outputs. In doing so, our RS-RAG framework effectively bridges the gap between remote sensing imagery and external knowledge sources, establishing a retrieval-augmented generation paradigm tailored to the unique demands of the remote sensing domain.

V. EXPERIMENTS

A. Experimental Setup

All input images are resized to 512 by 512 pixels before being fed into the models. We evaluate several state-of-the-art vision-language models as baselines, including InternVL2.5-Instruct-8B [29], Janus-Pro-7B [30], Qwen-2.5-VL-7B-Instruct [31], and LLaMA-3.2-Vision-11B-Instruct [32]. Building upon Qwen-2.5-VL and LLaMA-3.2-Vision, we further develop our retrieval-augmented variants, named RS-RAG-7B and RS-RAG-11B, respectively. To better adapt these models to the remote sensing domain, we fine-tune them via Low-Rank Adaptation (LoRA) [33] using instruction-following data consisting of 1380 curated image-text pairs. Fine-tuning is conducted for 3 epochs with a batch size of 1, using the Adamw optimizer and an initial learning rate of 1×10^{-4} . To systematically evaluate instruction-tuned vision-language models in the remote sensing domain, we curate a new benchmark consisting of task-specific subsets for image captioning (348 samples), image classification (910 samples), and visual question answering (300 samples). All experiments



Fig. 4. Qualitative results of image captioning on remote sensing imagery of the Great Seto Bridge. Text in red indicates the recognized landmark name; purple highlights retrieved world knowledge, such as historical, geographic, or cultural facts; and green denotes domain-specific knowledge, including spectral indices, land cover, and ALBEDO values.

TABLE III
PERFORMANCE COMPARISON BETWEEN BASELINE MODELS AND OUR PROPOSED RS-RAG VARIANTS ON THE IMAGE CAPTIONING TASK USING A SUBSET OF THE RSWK DATASET.

Model	BLEU-1	BLEU-2	BLEU-3	BLEU-4	METEOR	ROUGE-L	CIDEr
InternVL2.5-8B [29]	0.427	0.289	0.218	0.166	0.222	0.275	0.013
Janus-Pro-7B [30]	0.370	0.245	0.183	0.139	0.197	0.246	0.007
Qwen2.5-VL-7B [31]	0.349	0.223	0.161	0.121	0.185	0.229	0.004
Llama3.2-Vision-11B [32]	0.448	0.303	0.228	0.173	0.225	0.286	0.014
RS-RAG-7B	0.409	0.263	0.193	0.144	0.206	0.240	0.065
RS-RAG-11B	0.470	0.360	0.307	0.266	0.276	0.322	0.027

are performed using 3 NVIDIA RTX A6000 GPUs, each with 48 GB of memory.

To comprehensively evaluate model performance, we adopt a set of standard metrics tailored to each task. For image captioning and visual question answering, we report BLEU 1, BLEU 2, BLEU 3, BLEU 4, METEOR, ROUGE L, and CIDEr to measure the fluency, relevance, and informativeness of generated text. For the classification task, we evaluate both overall accuracy and per class accuracy to reflect model performance across diverse scene categories.

B. Results on Image Captioning Task

Table III summarizes the performance of baseline and proposed models on the image captioning task over remote sensing imagery, evaluated using a comprehensive set of metrics including BLEU-1 to BLEU-4, METEOR, ROUGE-L, and CIDEr. Among the baseline models, LLaMA3.2-Vision-11B achieves the strongest performance, attaining a BLEU-4 score of 0.173 and METEOR of 0.225, highlighting its relative strength in generating syntactically and semantically coherent captions. However, it still exhibits limitations in domain-specific understanding and factual richness due to its lack of grounding in external knowledge. In contrast, both of our proposed retrieval-augmented models, RS-RAG-7B and

TABLE IV
PERFORMANCE COMPARISON BETWEEN BASELINE MODELS AND OUR PROPOSED RS-RAG VARIANTS ON THE IMAGE CLASSIFICATION TASK USING A SUBSET OF THE RSWK DATASET.

Model	Overall Accuracy	Airport	Amusement Park	Beach	Bridge	Casino	Church	Gov. Bldg.	Historic Site	Mansion	Museum	Park	Stadium	Theater	Tower	University
InternVL2.5-8B [29]	0.329	0.959	0.250	0.667	0.385	0.000	0.000	0.152	0.158	0.023	0.000	0.672	0.790	0.039	0.053	0.654
Janus-Pro-7B [30]	0.269	0.959	0.500	0.778	0.308	0.000	0.480	0.485	0.061	0.000	0.000	0.373	0.632	0.000	0.053	0.161
Qwen2.5-VL-7B [31]	0.309	0.959	0.300	0.556	0.615	0.091	0.112	0.364	0.094	0.023	0.016	0.709	0.790	0.039	0.158	0.296
Llama3.2-Vision-11B [32]	0.340	0.959	0.300	0.667	0.462	0.091	0.020	0.061	0.052	0.047	0.278	0.746	0.816	0.039	0.053	0.568
RS-RAG-7B	0.659	0.959	0.800	0.667	0.692	0.636	0.551	0.576	0.474	0.419	0.349	0.866	0.868	0.346	0.368	0.765
RS-RAG-11B	0.842	0.980	0.900	0.944	0.769	0.727	0.820	0.849	0.655	0.512	0.714	0.843	0.842	0.769	0.526	0.803

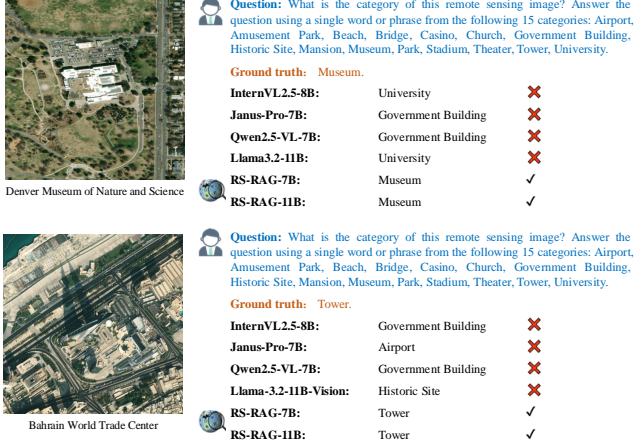


Fig. 5. Qualitative results of baseline models and our RS-RAG model on the image classification task using the RSWK dataset.

RS-RAG-11B, demonstrate consistent improvements across all evaluation metrics. Notably, RS-RAG-11B outperforms all baselines with a BLEU-4 of 0.266 and METEOR of 0.276, representing absolute gains of +0.093 and +0.051 over the strongest baseline. It also achieves the highest ROUGE-L score of 0.322, indicating improved phrase-level overlap with human-written descriptions. While RS-RAG-7B uses a smaller backbone, it still yields a significant performance boost, achieving the best CIDEr score of 0.065, which suggests enhanced alignment with human judgment of caption quality.

To better understand the effectiveness of our RS-RAG framework, we conduct a qualitative comparison of image captioning outputs generated by baseline models and our RS-RAG model, as shown in Fig. 4. The selected case depicts the Great Seto Bridge, a large-scale landmark in Japan. Baseline models, such as InternVL2.5-8B and Qwen2.5-VL-7B, either misidentify the landmark (e.g., predicting the Rainbow Bridge or Akashi Kaikyo Bridge) or generate overly generic descriptions without domain-grounded facts. Although LLaMA3.2-Vision-11B produces a correct name, it lacks detailed evidence from the image or environmental context. Notably, our proposed RS-RAG-7B and RS-RAG-11B models generate accurate, entity-aware, and knowledge-rich descriptions that correctly identify the Great Seto Bridge and provide factual details about its coordinates, construction history, and structural type. Furthermore, the descriptions include domain-specific knowledge (e.g., surface albedo, emissivity, and land cover classification), demonstrating the ability of our models to integrate retrieved remote sensing metadata. The use of world

knowledge, such as historical background and engineering facts, further enhances the semantic richness and correctness of the generated captions. These results highlight the benefits of retrieval-augmented generation in grounding VLM outputs with both domain and general-purpose knowledge.

C. Results on Image Classification Task

Table IV reports the performance of all models on the image classification task using a subset of the RSWK dataset, measured by overall accuracy and per-class accuracy across 15 scene categories. Among the baselines, LLaMA-3.2-Vision-11B achieves the highest overall accuracy at 34.0 percent, followed closely by InternVL2.5-8B and Qwen2.5-VL-7B. Despite these results, baseline models perform poorly on several knowledge-dependent categories such as Church, Mansion, Historic Site, and Museum, indicating their limited capacity to reason about semantically nuanced or infrequent classes. Our RS-RAG-11B model achieves a substantial improvement, attaining 84.2 percent overall accuracy. It outperforms all baselines by a large margin across nearly all categories, including challenging ones like Church with 82.0 percent accuracy and Historic Site with 65.5 percent accuracy. RS-RAG-7B also surpasses all baselines, reaching 65.9 percent overall accuracy, despite using a smaller backbone. These results demonstrate the effectiveness of integrating retrieved world and domain knowledge, which helps the model resolve semantic ambiguities and enhances recognition of visually similar or context-dependent categories in remote sensing imagery. To better understand the effectiveness of our RS-RAG framework, we conduct a qualitative comparison of image classification outputs generated by baseline models and our RS-RAG variants, as shown in Fig. 5. The figure presents two representative examples from the RSWK dataset: the Denver Museum of Nature and Science and the Bahrain World Trade Center. In both cases, existing vision-language baselines misclassify the scene, assigning incorrect labels such as "University," "Government Building," or "Historic Site." In contrast, RS-RAG-7B and RS-RAG-11B correctly identify the ground-truth categories, demonstrating a better understanding of scene semantics. These results qualitatively highlight the strength of retrieval-augmented generation in capturing contextual cues and leveraging external knowledge to improve fine-grained classification in complex remote sensing scenarios.

D. Results on Visual Question Answering Task

Table V presents the quantitative evaluation of various models on the VQA task using a subset of the RSWK dataset.

TABLE V
PERFORMANCE COMPARISON BETWEEN BASELINE MODELS AND OUR PROPOSED RS-RAG VARIANTS ON THE IMAGE VQA TASK USING A SUBSET OF THE RSWK DATASET

Model	BLEU-1	BLEU-2	BLEU-3	BLEU-4	METEOR	ROUGE-L	CIDEr
InternVL2.5-8B [29]	0.170	0.106	0.073	0.051	0.130	0.178	0.204
Janus-Pro-7B [30]	0.101	0.060	0.039	0.025	0.113	0.124	0.084
Qwen2.5-VL-7B [31]	0.116	0.067	0.042	0.026	0.124	0.135	0.105
Llama3.2-Vision-11B [32]	0.092	0.056	0.037	0.024	0.114	0.115	0.064
RS-RAG-7B	0.233	0.179	0.144	0.113	0.214	0.258	0.608
RS-RAG-11B	0.250	0.197	0.161	0.128	0.249	0.266	0.536

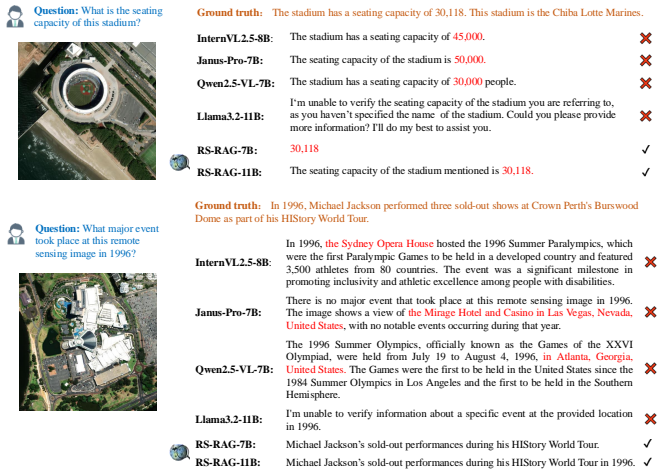


Fig. 6. Qualitative results of baseline models and our RS-RAG model on the VQA task using the RSWK dataset.

Across all metrics—including BLEU, METEOR, ROUGE-L, and CIDEr—the proposed RS-RAG variants outperform all baselines by substantial margins. RS-RAG-11B achieves the highest scores on BLEU-1, BLEU-4, and METEOR, indicating more fluent and semantically relevant answers. RS-RAG-7B also delivers competitive results, achieving the best CIDEr score of 0.608, suggesting strong alignment with human-annotated answers in terms of informativeness and precision. In contrast, baseline models such as Qwen2.5-VL-7B and Janus-Pro-7B struggle to generate accurate or coherent responses, especially in knowledge-intensive queries. To better understand the sources of these improvements, Fig. 6 illustrates two representative qualitative examples. In the first case, the model is asked about the seating capacity of a stadium. Baseline responses are either factually incorrect or overly generic, whereas both RS-RAG models retrieve and accurately generate the correct capacity of 30,118. In the second example, involving a historically grounded question, only RS-RAG models correctly identify Michael Jackson’s concerts at Burswood Dome during his HIStory World Tour in 1996. Other models either hallucinate unrelated content, such as the 1996 Summer Olympics, or fail to recognize the event entirely. These examples underscore the strength of RS-RAG in incorporating relevant domain and world knowledge to produce accurate, informative, and context-aware answers in remote sensing VQA tasks.

E. Ablation Studies

Effect of the number of retrieved candidates. To investigate the impact of the number of retrieved candidates in the retrieval-augmented generation process, we conduct an ablation study on the top- k parameter in RS-RAG, as shown in Table VI. With the fusion weight α in Eq.7 fixed to 0.9, we evaluate the model’s performance on the image captioning task under different values of k . The results show that retrieving a single, highly relevant knowledge snippet ($k = 1$) yields the best performance across all evaluation metrics. As k increases to 3 and 5, the performance consistently degrades, indicating that incorporating more candidates introduces semantic redundancy or irrelevant noise. Such noise can interfere with the model’s ability to generate concise and accurate captions. These findings underscore the importance of retrieval precision in the remote sensing domain and confirm that fewer, but higher-quality, knowledge segments are more effective for guiding the generation process.

TABLE VI
ABLATION STUDY ON THE NUMBER OF TOP- k RETRIEVED CANDIDATES FOR RS-RAG.

Top- k	BLEU-1	BLEU-2	BLEU-3	BLEU-4	METEOR	ROUGE-L	CIDEr
$k = 1$	0.562	0.449	0.385	0.336	0.308	0.362	0.072
$k = 3$	0.458	0.339	0.278	0.232	0.257	0.283	0.044
$k = 5$	0.433	0.314	0.255	0.210	0.244	0.271	0.063

Effect of fusion weight α . We further explore the effect of the fusion weight α that balances visual and textual similarity in the re-ranking step (see Eq.7). Table VII reports performance under different values of α , with the number of retrieved candidates fixed to $k = 1$. The results show that $\alpha = 0.5$ achieves the best overall performance, indicating that equal weighting of visual and text similarity provides the most informative guidance for downstream caption generation. When α is too low (e.g., 0.3), text similarity dominates, leading to less visually grounded results. Conversely, when α increases beyond 0.5, performance slightly degrades, suggesting that over-reliance on visual similarity may overlook relevant textual semantics. These findings confirm that effective cross-modal fusion is critical for high-quality retrieval and generation.

VI. CONCLUSION

In this work, we presented RS-RAG, a retrieval-augmented vision-language framework designed to bridge remote sensing imagery with structured domain and world knowledge. To

TABLE VII
ABLATION STUDY ON THE FUSION WEIGHT α IN RS-RAG.

α	BLEU-1	BLEU-2	BLEU-3	BLEU-4	METEOR	ROUGE-L	CIDEr
0.3	0.414	0.253	0.179	0.127	0.215	0.199	0.005
0.5	0.582	0.473	0.410	0.361	0.318	0.393	0.210
0.7	0.568	0.454	0.389	0.338	0.309	0.366	0.110
0.9	0.562	0.449	0.385	0.336	0.308	0.362	0.072

support this framework, we constructed the RSWK dataset, a large-scale multimodal benchmark that integrates high-resolution satellite imagery with rich textual descriptions covering over 14,000 globally recognized locations from 175 countries. By leveraging this curated knowledge base, RS-RAG significantly improves contextual reasoning and semantic understanding across key vision-language tasks, including image captioning, image classification, and visual question answering. Extensive experiments validate the effectiveness of our approach, particularly in handling complex, knowledge-intensive queries. We believe that both the RSWK dataset and the RS-RAG framework provide a strong foundation for advancing research in remote sensing vision-language understanding and knowledge-grounded geospatial AI.

REFERENCES

- [1] W. Han, C. Wen, L. Chok, Y. L. Tan, S. L. Chan, H. Zhao, and C. Feng, "Autoencoding tree for city generation and applications," *ISPRS Journal of Photogrammetry and Remote Sensing*, vol. 208, pp. 176–189, 2024.
- [2] S. Liu, S. Wang, T. Chi, C. Wen, T. Wu, and D. Wang, "An improved combined vegetation difference index and burn scar index approach for mapping cropland burned areas using combined data from landsat 8 multispectral and thermal infrared bands," *International Journal of Wildland Fire*, vol. 29, no. 6, pp. 499–512, 2020.
- [3] C. Wen, S. Liu, X. Yao, L. Peng, X. Li, Y. Hu, and T. Chi, "A novel spatiotemporal convolutional long short-term neural network for air pollution prediction," *Science of the total environment*, vol. 654, pp. 1091–1099, 2019.
- [4] X. X. Zhu, D. Tuia, L. Mou, G.-S. Xia, L. Zhang, F. Xu, and F. Fraundorfer, "Deep learning in remote sensing: A comprehensive review and list of resources," *IEEE Geoscience and Remote Sensing Magazine*, vol. 5, no. 4, pp. 8–36, 2017.
- [5] H. Lin, N. Li, P. Yao, K. Dong, Y. Guo, D. Hong, Y. Zhang, and C. Wen, "Generalization-enhanced few-shot object detection in remote sensing," *IEEE Transactions on Circuits and Systems for Video Technology*, 2025.
- [6] Y. Hu, J. Yuan, C. Wen, X. Lu, and X. Li, "Rsgpt: A remote sensing vision language model and benchmark," *arXiv preprint arXiv:2307.15266*, 2023.
- [7] Y. Bazi, L. Bashmal, M. M. Al Rahhal, R. Ricci, and F. Melgani, "Rs-llava: A large vision-language model for joint captioning and question answering in remote sensing imagery," *Remote Sensing*, vol. 16, no. 9, p. 1477, 2024.
- [8] C. Pang, J. Wu, J. Li, Y. Liu, J. Sun, W. Li, X. Weng, S. Wang, L. Feng, G.-S. Xia, and C. He, "H2rsvlm: Towards helpful and honest remote sensing large vision language model," 2024.
- [9] W. Zhang, M. Cai, T. Zhang, Y. Zhuang, and X. Mao, "Earthgpt: A universal multi-modal large language model for multi-sensor image comprehension in remote sensing domain," *IEEE Transactions on Geoscience and Remote Sensing*, 2024.
- [10] K. Kuckreja, M. S. Danish, M. Naseer, A. Das, S. Khan, and F. S. Khan, "Geochat: Grounded large vision-language model for remote sensing," in *Proceedings of the IEEE/CVF Conference on Computer Vision and Pattern Recognition*, 2024, pp. 27 831–27 840.
- [11] Y. Zhan, Z. Xiong, and Y. Yuan, "Skyeyegpt: Unifying remote sensing vision-language tasks via instruction tuning with large language model," *ISPRS Journal of Photogrammetry and Remote Sensing*, vol. 221, pp. 64–77, 2025.
- [12] S. Lobry, D. Marcos, J. Murray, and D. Tuia, "Rsvqa: Visual question answering for remote sensing data," *IEEE Transactions on Geoscience and Remote Sensing*, vol. 58, no. 12, pp. 8555–8566, 2020.
- [13] X. Zheng, B. Wang, X. Du, and X. Lu, "Mutual attention inception network for remote sensing visual question answering," *IEEE Transactions on Geoscience and Remote Sensing*, vol. 60, pp. 1–14, 2021.
- [14] Y. Sun, S. Feng, X. Li, Y. Ye, J. Kang, and X. Huang, "Visual grounding in remote sensing images," in *Proceedings of the 30th ACM International conference on Multimedia*, 2022, pp. 404–412.
- [15] M. M. Al Rahhal, Y. Bazi, S. O. Alsaleh, M. Al-Razgan, M. L. Mekhalif, M. Al Zuair, and N. Alajlan, "Open-ended remote sensing visual question answering with transformers," *International Journal of Remote Sensing*, vol. 43, no. 18, pp. 6809–6823, 2022.
- [16] Y. Zhan, Z. Xiong, and Y. Yuan, "Rsvg: Exploring data and models for visual grounding on remote sensing data," *IEEE Transactions on Geoscience and Remote Sensing*, vol. 61, pp. 1–13, 2023.
- [17] B. Qu, X. Li, D. Tao, and X. Lu, "Deep semantic understanding of high resolution remote sensing image," in *2016 International conference on computer, information and telecommunication systems (Cits)*. IEEE, 2016, pp. 1–5.
- [18] X. Lu, B. Wang, X. Zheng, and X. Li, "Exploring models and data for remote sensing image caption generation," *IEEE Transactions on Geoscience and Remote Sensing*, vol. 56, no. 4, pp. 2183–2195, 2017.
- [19] Z. Zhang, T. Zhao, Y. Guo, and J. Yin, "Rs5m and georsclip: A large scale vision-language dataset and a large vision-language model for remote sensing," *IEEE Transactions on Geoscience and Remote Sensing*, 2024.
- [20] F. Liu, D. Chen, Z. Guan, X. Zhou, J. Zhu, Q. Ye, L. Fu, and J. Zhou, "Remotclip: A vision language foundation model for remote sensing," *IEEE Transactions on Geoscience and Remote Sensing*, 2024.
- [21] H. Lin, C. Zhang, D. Hong, K. Dong, and C. Wen, "Fedrsclip: Federated learning for remote sensing scene classification using vision-language models," *arXiv preprint arXiv:2501.02461*, 2025.
- [22] X. Li, C. Wen, Y. Hu, Z. Yuan, and X. X. Zhu, "Vision-language models in remote sensing: Current progress and future trends," *IEEE Geoscience and Remote Sensing Magazine*, 2024.
- [23] X. Li, C. Wen, Y. Hu, and N. Zhou, "Rs-clip: Zero shot remote sensing scene classification via contrastive vision-language supervision," *International Journal of Applied Earth Observation and Geoinformation*, 2023.
- [24] K. Kuckreja, M. S. Danish, M. Naseer, A. Das, S. Khan, and F. S. Khan, "Geochat: Grounded large vision-language model for remote sensing," in *Proceedings of the IEEE/CVF Conference on Computer Vision and Pattern Recognition*, 2024, pp. 27 831–27 840.
- [25] H. Lin, D. Hong, S. Ge, C. Luo, K. Jiang, H. Jin, and C. Wen, "Rs-moe: A vision-language model with mixture of experts for remote sensing image captioning and visual question answering," *IEEE Transactions on Geoscience and Remote Sensing*, 2025.
- [26] A. Hurst, A. Lerer, A. P. Goucher, A. Perelman, A. Ramesh, A. Clark, A. Ostrow, A. Welihinda, A. Hayes, A. Radford *et al.*, "Gpt-4o system card," *arXiv preprint arXiv:2410.21276*, 2024.
- [27] A. Liu, B. Feng, B. Xue, B. Wang, B. Wu, C. Lu, C. Zhao, C. Deng, C. Zhang, C. Ruan *et al.*, "Deepseek-v3 technical report," *arXiv preprint arXiv:2412.19437*, 2024.
- [28] Q. Zhao, L. Yu, X. Li, D. Peng, Y. Zhang, and P. Gong, "Progress and trends in the application of google earth and google earth engine," *Remote Sensing*, vol. 13, no. 18, p. 3778, 2021.
- [29] Z. Chen, J. Wu, W. Wang, W. Su, G. Chen, S. Xing, M. Zhong, Q. Zhang, X. Zhu, L. Lu *et al.*, "Internvl: Scaling up vision foundation models and aligning for generic visual-linguistic tasks," in *Proceedings of the IEEE/CVF Conference on Computer Vision and Pattern Recognition*, 2024, pp. 24 185–24 198.
- [30] X. Chen, Z. Wu, X. Liu, Z. Pan, W. Liu, Z. Xie, X. Yu, and C. Ruan, "Janus-pro: Unified multimodal understanding and generation with data and model scaling," *arXiv preprint arXiv:2501.17811*, 2025.
- [31] Q. Team, "Qwen2.5-vl," January 2025. [Online]. Available: <https://qwenlm.github.io/blog/qwen2.5-vl/>
- [32] M. AI, "Llama 3.2: Revolutionizing edge ai and vision with open-source models," 2024. [Online]. Available: <https://ai.meta.com/blog/llama-3-2-connect-2024-vision-edge-mobile-devices/>
- [33] E. J. Hu, Y. Shen, P. Wallis, Z. Allen-Zhu, Y. Li, S. Wang, L. Wang, W. Chen *et al.*, "Lora: Low-rank adaptation of large language models," *ICLR*, vol. 1, no. 2, p. 3, 2022.